

Jantzen T., Hack K., Yazhenskikh E., Müller M.  
 Chimica Techno Acta. 2018. Vol. 5, No. 4. P. 166–188.  
 ISSN 2409–5613

**T. Jantzen<sup>a</sup>, K. Hack<sup>a</sup>, E. Yazhenskikh<sup>b</sup>, M. Müller<sup>b</sup>**

<sup>a</sup> GTT-Technologies, Kaiserstraße 103, D-52134 Herzogenrath, Germany

<sup>b</sup> Forschungszentrum Jülich GmbH, IEK-2, D-52425 Jülich, Germany

E-mail: [tj@gtt-technologies.de](mailto:tj@gtt-technologies.de)

## Thermodynamic assessment of oxide system $\text{In}_2\text{O}_3\text{-SnO}_2\text{-ZnO}$

The  $\text{In}_2\text{O}_3\text{-SnO}_2\text{-ZnO}$  system is of special interest for applications as transparent conducting oxides and also transparent semiconductors. In the present work, a thermodynamic assessment for this system is discussed using all available experimental data on phase equilibria and thermodynamic properties. All subsystems including elemental combinations were considered in order to generate a self-consistent Gibbs energy dataset for further calculation and prediction of thermodynamic properties of the system. The modified associate species model was used for the description of the liquid phase. Particular attention was given to two significant solid solution phases: Spinel with the formula  $\text{Zn}_{(2-x)}\text{Sn}_{(1-x)}\text{In}_{2x}\text{O}_4$  based on  $\text{Zn}_2\text{SnO}_4$  and Bixbyite based on  $\text{In}_2\text{O}_3$  and extending strongly toward the  $\text{SnZnO}_3$  composition according to the formula  $\text{In}_{(2-2x)}\text{Sn}_x\text{Zn}_x\text{O}_3$ . In addition to the component oxides, nine quasi-binary compounds located in the  $\text{In}_2\text{O}_3\text{-ZnO}$  binary subsystem have also been included in the database as stoichiometric phases.

**Keywords:** phase diagram; thermodynamic modeling; indium oxide; bixbyite; spinel

Received: 28.11.2018. Accepted: 14.12.2018. Published: 31.12.2018.

© Jantzen T., Hack K., Yazhenskikh E., Müller M., 2018

### Introduction

Compositions in the  $\text{In}_2\text{O}_3\text{-SnO}_2\text{-ZnO}$  ternary oxide system are of interest owing to their optical transparency combined with high electrical conductivity [1, 2]. Transparent conducting oxides (TCOs) can be used as electrodes in solar cells, flat panel displays and other commercial devices. Although TCOs are applied usually in film form, the study of bulk phase relations and physical properties can be useful for understanding fundamental materials properties. At the present time, ITO (tin-doped indium oxide) is the material of choice for TCO layers (e.g. in review [3]), but the increasing cost of indium metal and the development of new tech-

nologies will require alternative TCOs. According to Palmer [4] both  $\text{SnO}_2$  and  $\text{ZnO}$  are good TCOs with conductivities comparable to ITO. Compositions from the  $\text{In}_2\text{O}_3\text{-ZnO}$  system with high Zn concentration are attractive due to their high electrical conductivity, optical transparency and excellent chemical stability [5, 6].

The materials from the system ZITO (Zn-In-Sn-O) [2] are promising replacements for ITO as TCO layers in many opto-electronic applications. ZITO contains less indium than ITO, which lowers the cost, and it has a broad window of compositions that allow the TCO layer to be adjusted (conductivity, etc.) for each

application. The bulk equilibrium phases of ZITO have been defined and exhibit two transparent and conductive regions: the bixbyite solid solution  $\text{In}_{2-2x}\text{Zn}_x\text{Sn}_x\text{O}_3$  and the homologous series of compounds  $\text{In}_2\text{Zn}_k\text{O}_{k+3}$ .

Thermodynamic modelling on the basis of reliable experimental data and appropriate Gibbs energy models for solid and liquid phases is a powerful tool for calculation and prediction of the thermodynamic properties and phase equilibria for various systems. Furthermore, such data can be applied for heat balance calculations, i.e. for information on the energetics of possible production processes. The quality and completeness of the thermodynamic databases used is a key prerequisite for reliable calculations. According to CALPHAD-type modelling all available experimental data (phase equilibria, mixing properties, component activities, etc.) are critically analyzed in terms of their consistency. Each phase in the system is treated by an appropriate Gibbs energy model with adjustable parameters (Gibbs energy of constituents, interaction parameters, etc.), which are optimized in accordance with the experimental information in order to generate a self-consistent dataset of Gibbs energies of all phases in a system.

In the present study the thermodynamic assessment of the oxide system  $\text{In}_2\text{O}_3\text{-SnO}_2\text{-ZnO}$  is presented using all available experimental data on phase equilibria and thermodynamic properties. The

### Thermodynamic models

The Gibbs energies of the elements were taken from the SGTE unary database [11] while the pure component oxides were taken from the SGTE Pure Substance database [12], the thermodynamic descriptions of the metallic systems were taken

calculation of phase equilibria and the prediction of thermodynamic properties using the database for the  $\text{In}_2\text{O}_3\text{-SnO}_2\text{-ZnO}$  system can be helpful for developing and manufacturing TCOs for optoelectronic devices. The experimental information on the available thermodynamic properties (phase diagram, phase transition etc.) is used for the generation of self-consistent Gibbs energy datasets for all known phases and compounds in this ternary system.

The Gibbs energy of the liquid phase has been modelled using a non-ideal associate solution model proposed by Bessmann and Spear [7]. This model has been successfully applied for the description of melts containing oxides and sulphides in our previous studies, e.g. in [8–10]. Solubilities in the solid state have been treated using the multi-sublattice approach which allows the description of experimentally determined solubilities. In the present study there are two solid solution series with different structure. The spinel phase with formula  $(\text{Zn}^{+2}, \text{In}^{+3})_2(\text{Sn}^{+4}, \text{Zn}^{+2})_4(\text{O}^{2-})_4$  includes  $\text{Zn}_2\text{SnO}_4$ ,  $\text{In}_2\text{SnO}_4$ ,  $\text{Zn}_2\text{ZnO}_4$ ,  $\text{In}_2\text{ZnO}_4$  as end-members. The model for bixbyite in form of  $\text{In}_{(2-2x)}\text{Sn}_x\text{Zn}_x\text{O}_3$  using the formula  $(\text{In}, \text{Zn}, \text{Va})_1(\text{In}, \text{Sn})_1(\text{O})_3$  allows description of the limited solubility from pure indium oxide extending to  $\text{SnZn}$  compounds.

The present database contains a gas phase, a multi-component liquid phase, 7 solid solutions and 27 solid stoichiometric compounds.

from the SGTE Solution database [13]. The thermodynamic data sources used in the present work are collected in Table 1.

The thermodynamic descriptions of the assessed stoichiometric compounds are presented in Table 2.

Table 1

Thermodynamic data sources used in present work

System	Source	System	Source
In-Sn	[13]	In <sub>2</sub> O <sub>3</sub> -SnO <sub>2</sub>	This work
In-Zn	[13]	In <sub>2</sub> O <sub>3</sub> -ZnO	This work
Sn-Zn	[13]	SnO <sub>2</sub> -ZnO	This work
In-O	This work	In <sub>2</sub> O <sub>3</sub> -SnO <sub>2</sub> -ZnO	This work
Sn-O	This work	-	-
Zn-O	This work	-	-

The solid solution phases in the In<sub>2</sub>O<sub>3</sub>-SnO<sub>2</sub>-ZnO system considered in the present work are given in Table 3 and are described below in more detail.

### The molten oxide phase

The Gibbs energy of the liquid phase in the system is represented by the modified non-ideal associate species model [7]. The basic species In<sub>2</sub>O<sub>3</sub>, SnO<sub>2</sub> and ZnO along with one (quasi)binary species (SnZn<sub>2</sub>O<sub>4</sub>) have been introduced as liquid components. Although the corresponding metallic species were added for the systems Me-O, the present work will attend to the melt oxide species only; the interactions between these oxides and other oxide species are responsible for the thermodynamic properties of the liquid phase. To provide equal weighting of each associate species with regard to its entropic contribution in the ideal mixing term, each species contains a total of two cations in its formula based on [7]. In addition, interactions between associate species were introduced in order to fine tune the thermodynamic description.

The molar Gibbs energy of the solution is presented by a three-term expression with contributions of the reference part, the ideal and the excess part taking into account binary interactions as follows:

$$G_m = \sum x_i {}^\circ G_i + RT \sum x_i \ln x_i + \sum_{i < j} \sum_{v=0} L_{ij}^{(v)} (x_i - x_j)^v \quad (1)$$

where  $x_i$  is the mole fraction of phase constituent  $i$  (including the associate species),  ${}^\circ G_i$  is the molar Gibbs energy of the pure phase constituent  $i$  and  $L_{ij}$  is an interaction coefficient between components  $i$  and  $j$ , according to the Redlich — Kister polynomial. The  $L_{ij}^{(v)}$  with  $v = 0, 1, 2$  and  ${}^\circ G_i$  are temperature dependent in the same way according to:

$${}^\circ G_i, L_{ij}^{(v)} = A + B \cdot T + c \cdot T \cdot \ln(T) + D \cdot T^2 + E \cdot T^{-1} + F \cdot T^3 \quad (2)$$

Thermodynamic data for the liquid components are summarized in Table 3. The elemental systems In-O and Zn-O contain one stable oxide, In<sub>2</sub>O<sub>3</sub> and ZnO, respectively, while in the system Sn-O two oxides were considered, Sn<sub>2</sub>O<sub>2</sub> and Sn<sub>2</sub>O<sub>4</sub>. The liquid phase of the quasi-binary oxide systems will contain the basic oxides along with one (quasi)binary species (SnZn<sub>2</sub>O<sub>4</sub> · 3/2). No ternary species were necessary. The Gibbs energy of the binary species are taken from the SGTE Pure Substance database [12] without modifications. The G function of the liquid species SnZn<sub>2</sub>O<sub>4</sub> · 3/2 was derived using the melting data of the

Table 2

Thermodynamic properties of stoichiometric compounds assessed in this work

Compound	$\Delta_f H^{298}$ , J/mol	$S_{298}^0$ , J/mol · K	T (K)	$C_p$ , J/mol·K
SnO	-289853	48.95	298–1250	$43.7399+0.01356023 \cdot T + 10 \cdot T^{-2} - 1.06 \cdot 10^{-10} \cdot T^2$ [13]
Sn <sub>3</sub> O <sub>4</sub>	-1155713	151.23	298–1250	$163.5208+0.03448263 \cdot T - 2223847 \cdot T^{-2} + 5.57 \cdot 10^{-10} \cdot T^2$
SnIn <sub>2</sub> O <sub>5</sub>	-1439306.47	187.51	298–1903	$197.5511+0.01742532 \cdot T - 4485329 \cdot T^{-2} + 3.968488 \cdot 10^{-10} \cdot T^2$
			1903–2186	$213.5101 + 0.01006315 \cdot T - 2261462 \cdot T^{-2} - 3.721512 \cdot 10^{-10} \cdot T^2$
Sn <sub>3</sub> In <sub>4</sub> O <sub>12</sub>	-3458277.2	426.23	298–1903	$471.1432+0.04221281 \cdot T - 11194525 \cdot T^{-2} + 3.968488 \cdot 10^{-10} \cdot T^2$
			1903–2186	$213.5101 + 0.01006315 \cdot T - 2261462 \cdot T^{-2} + 1.5626976 \cdot 10^{-9} \cdot T^2$
Zn <sub>3</sub> In <sub>2</sub> O <sub>6</sub>	-1975291.24	231.8	298–2186	$264.2621+0.02177245 \cdot T - 4512542 \cdot T^{-2} + 3.8375878488 \cdot 10^{-6} \cdot T^2$
Zn <sub>4</sub> In <sub>2</sub> O <sub>7</sub>	-2326518.2	274.79	298–2186	$311.8461+0.02567555 \cdot T - 4512542 \cdot T^{-2} + 3.8375878488 \cdot 10^{-6} \cdot T^2$
Zn <sub>3</sub> In <sub>2</sub> O <sub>8</sub>	-2678001	317.6	298–2186	$359.4301+0.02957865 \cdot T - 6013262 \cdot T^{-2} + 6.3962278488 \cdot 10^{-6} \cdot T^2$
Zn <sub>6</sub> In <sub>2</sub> O <sub>9</sub>	-3028592	360.86	298–2186	$407.0141+0.03348175 \cdot T - 6763622 \cdot T^{-2} + 7.6755478488 \cdot 10^{-6} \cdot T^2$
Zn <sub>7</sub> In <sub>2</sub> O <sub>10</sub>	-3379500	403.92	298–2186	$454.5981+0.03738485 \cdot T - 7513982 \cdot T^{-2} + 8.9548678488 \cdot 10^{-6} \cdot T^2$
Zn <sub>9</sub> In <sub>2</sub> O <sub>12</sub>	-4080212	490.44	298–2186	$549.7661+0.04519105 \cdot T - 9014702 \cdot T^{-2} + 1.15135078488 \cdot 10^{-5} \cdot T^2$
Zn <sub>11</sub> In <sub>2</sub> O <sub>14</sub>	-4781168.4	576.79	298–2186	$644.9341+0.05299725 \cdot T - 10515422 \cdot T^{-2} + 1.40721478488 \cdot 10^{-5} \cdot T^2$
Zn <sub>13</sub> In <sub>2</sub> O <sub>16</sub>	-5482137.2	663.13	298–2186	$644.9341+0.05299725 \cdot T - 10515422 \cdot T^{-2} + 1.40721478488 \cdot 10^{-5} \cdot T^2$
Zn <sub>15</sub> In <sub>2</sub> O <sub>18</sub>	-6183104.984	749.4702	298–2186	$835.2701+0.06860965 \cdot T - 13516862 \cdot T^{-2} + 1.91894278488 \cdot 10^{-5} \cdot T^2$
SnZn <sub>2</sub> O <sub>4</sub>	-1282630	151	298–1903	$171.209+0.01516837 \cdot T - 3724587 \cdot T^{-2} + 2.55940900002 \cdot 10^{-6} \cdot T^2$
			1903–2250	$187.168+0.0078062 \cdot T - 1500720 \cdot T^{-2} + 2.55864 \cdot 10^{-6} \cdot T^2$

corresponding constituent oxides. The interactions between liquid species are listed in Table 3.

### Spinel

Normal Spinel can be described using the formula  $AB_2O_4$ , where A is a divalent metallic cation and B represents a trivalent cation placed on the second sublattice. For example, zinc aluminate ( $ZnAl_2O_4$ ) and zinc ferrite ( $ZnFe_2O_4$ ) are normal spinels. On the other hand, zinc stannate  $Zn_2SnO_4$

is an inverse spinel and has the chemical formula  $A_2BO_4$  where A are divalent zinc cations and B tetravalent tin cations, as in  $(Zn^{2+})_2(Sn^{4+})(O^{2-})_4$ . The inverse Spinel  $Zn_2SnO_4$  has the cubic spinel structure (space group ) and Pearson symbol  $cF56$  [14]. This inverse spinel structure is present in many systems, e.g. as Ülvöspinel  $Fe_2TiO_4$ , manganese titanate  $Mn_2TiO_4$  and gandilite  $Mg_2TiO_4$ . All of them can be treated with the same common formula

Table 3

Thermodynamic descriptions of the liquid and solid solution phases	
Parameter value, J/mol	Reference
Liquid: (In, In <sub>2</sub> O <sub>3</sub> , Sn, Sn <sub>2</sub> O <sub>2</sub> , Sn <sub>2</sub> O <sub>4</sub> , Zn, Zn <sub>2</sub> O <sub>2</sub> , SnZn <sub>2</sub> O <sub>4</sub> /1.5)	*
${}^\circ G_{In} = {}^\circ G_{Liq-In}^{SGPS}$	[11]
${}^\circ G_{In_2O_3} = {}^\circ G_{Liq-Ti_2O_3}^{SGPS}$	[12]
${}^\circ G_{Sn} = {}^\circ G_{Liq-Sn}^{SGPS}$	[11]
${}^\circ G_{Sn_2O_2} = 2{}^\circ G_{Liq-SnO}^{SGPS}$	[12]
${}^\circ G_{Sn_2O_4} = 2{}^\circ G_{Liq-SnO_2}^{SGPS}$	[12]
${}^\circ G_{Zn} = {}^\circ G_{Liq-Zn}^{SGPS}$	[11]
${}^\circ G_{SnZn_2O_4} = {}^\circ G_{SnZn_2O_4}^{Spinel} + 163400 - 80.81806 \cdot T$	*
${}^\circ L_{In, In_2O_3}^{liq} = +27600$	*
${}^\circ L_{Sn, SnO}^{liq} = +39000$	*
${}^1 L_{Sn, SnO}^{liq} = +11200$	*
${}^\circ L_{Sn, SnO_2}^{liq} = +44000$	*
${}^\circ L_{In_2O_3, SnO_2}^{liq} = -11000$	*
${}^\circ L_{In_2O_3, ZnO}^{liq} = -11000$	*
${}^\circ L_{In_2O_3, SnO_2, Sn}^{liq} = -187000$	*
Spinel: $(Zn^{2+}, Sn^{4+})_1(Zn^{2+}, In^{3+})_2(O^{2-})_4$	*
${}^\circ G_{Zn^{2+}:Zn^{2+}:O^{2-}} = 0.5 \cdot {}^\circ G_{SnZn_2O_4}^{Spinel} + 0.5 \cdot {}^\circ G_{ZnIn_2O_4}^{Spinel} + 9500$	*
${}^\circ G_{Zn^{2+}:In^{3+}:O^{2-}} = {}^\circ G_{ZnIn_2O_4}^{Spinel} = {}^\circ G_{ZnO}^{SGPS} + {}^\circ G_{In_2O_3}^{SGPS} + 27000$	*
${}^\circ G_{Sn^{4+}:Zn^{2+}:O^{2-}} = {}^\circ G_{SnZn_2O_4}^{Spinel}$	*
${}^\circ G_{Sn^{4+}:In^{3+}:O^{2-}} = 0.5 \cdot {}^\circ G_{SnZn_2O_4}^{Spinel} + 0.5 \cdot {}^\circ G_{ZnIn_2O_4}^{Spinel} + 9500$	*

Parameter value, J/mol	Reference
Bixbyite: $(\underline{\text{In}}, \text{Zn}, \text{Va})(\underline{\text{In}}, \text{Sn})(\text{O})_3$	*
${}^{\circ}G_{\text{In:In:O}} = {}^{\circ}G_{\text{In}_2\text{O}_3}^{\text{SGPS}}$	[12]
${}^{\circ}G_{\text{In:Sn:O}} = 0.5 \cdot {}^{\circ}G_{\text{In}_2\text{O}_3}^{\text{SGPS}} + 0.5 \cdot {}^{\circ}G_{\text{ZnSnO}_3}^{\text{Bixbyite}} + 20000 + 11 \cdot T$	*
${}^{\circ}G_{\text{Zn:In:O}} = 0.5 \cdot {}^{\circ}G_{\text{In}_2\text{O}_3}^{\text{SGPS}} + 0.5 \cdot {}^{\circ}G_{\text{ZnSnO}_3}^{\text{Bixbyite}} + 119044 - 3 \cdot T$	*
${}^{\circ}G_{\text{Zn:Sn:O}} = {}^{\circ}G_{\text{ZnSnO}_3}^{\text{Bixbyite}} = {}^{\circ}G_{\text{ZnO}}^{\text{SGPS}} + {}^{\circ}G_{\text{SnO}_2}^{\text{SGPS}} - 10800$	*
${}^{\circ}G_{\text{Va:In:O}} = 0.5 \cdot {}^{\circ}G_{\text{In}_2\text{O}_3}^{\text{SGPS}}$	*
${}^{\circ}G_{\text{Va:Sn:O}} = {}^{\circ}G_{\text{SnO}_2}^{\text{SGPS}} + 12000$	*
${}^0L_{\text{In:In,Sn:O}}^{\text{Bixbyite}} = -46403 + 13 \cdot T$	
${}^0L_{\text{In,Zn:In:O}}^{\text{Bixbyite}} = -10.52 \cdot T$	
${}^0L_{\text{In,Zn:Sn:O}}^{\text{Bixbyite}} = +1700$	
${}^0L_{\text{In,Zn:In,Sn:O}}^{\text{Bixbyite}} = -318000$	
${}^1L_{\text{In,Zn:In,Sn:O}}^{\text{Bixbyite}} = -97000$	

\* — This work.

$(\text{A}^{2+})_2(\text{B}^{4+})(\text{O}^{2-})_4$ . In the  $\text{In}_2\text{O}_3$ - $\text{SnO}_2$ - $\text{ZnO}$  ternary system the spinel phase  $\text{Zn}_2\text{SnO}_4$  dissolves a significant amount of indium and extends toward the fictive  $\text{ZnO} \cdot \text{In}_2\text{O}_3$  composition, having constant Zn:Sn ratio [1] according to the formula  $\text{Zn}_{(2-x)}\text{Sn}_{(1-x)}\text{In}_{2x}\text{O}_4$ . The proposed multi sublattice formula reads  $(\underline{\text{Zn}}^{2+}, \text{In}^{3+})_2(\underline{\text{Sn}}^{4+}, \text{Zn}^{2+})_1(\text{O}^{2-})_4$  and allows to describe the deviation from the stoichiometric composition towards higher  $\text{In}_2\text{O}_3$ -contents keeping the Zn:Sn ratio to 2:1.

The molar Gibbs energy of the phase Spinel was expressed using the compound energy formalism derived by Hillert and Staffansson [15] and generalized by Sundman and Ågren [16] under the condition  $y_{\text{O}^{2-}}^{\text{III}} = 1$  as follows:

$$G_m = y_{\text{Zn}^{2+}}^{\text{I}} y_{\text{Sn}^{4+}}^{\text{II}} {}^{\circ}G_{\text{Zn}_2\text{SnO}_4} + y_{\text{Zn}^{2+}}^{\text{I}} y_{\text{Zn}^{2+}}^{\text{II}} {}^{\circ}G_{\text{Zn}_2\text{ZnO}_4[2-]} +$$

$$+ y_{\text{In}^{3+}}^{\text{I}} y_{\text{Sn}^{4+}}^{\text{II}} {}^{\circ}G_{\text{In}_2\text{SnO}_4[2+]} + y_{\text{In}^{3+}}^{\text{I}} y_{\text{Zn}^{2+}}^{\text{II}} {}^{\circ}G_{\text{In}_2\text{ZnO}_4} + 2RT \left( y_{\text{Zn}^{2+}}^{\text{I}} \ln y_{\text{Zn}^{2+}}^{\text{I}} + y_{\text{In}^{3+}}^{\text{I}} \ln y_{\text{In}^{3+}}^{\text{I}} \right) + RT \left( y_{\text{Sn}^{4+}}^{\text{II}} \ln y_{\text{Sn}^{4+}}^{\text{II}} + y_{\text{Zn}^{2+}}^{\text{II}} \ln y_{\text{Zn}^{2+}}^{\text{II}} \right) + G_m^{\text{ex}} \quad (3)$$

where  $y_i^s$  represents the site fractions of sublattice component  $i$  on sublattice  $s$ .  ${}^{\circ}G_{i;j\text{O}^{2-}}$  are the Gibbs energy of real ( $\text{Zn}_2\text{SnO}_4$ ) or hypothetical compounds where the first and second sublattices are occupied by appropriate components  $i$  and  $j$ , is the excess Gibbs energy which depends on the site fractions  $y_i^N$  and on temperature.

### Bixbyite

Indium oxide  $\text{In}_2\text{O}_3$  exists in form of two crystalline phases, the cubic form (Bixbyite type like  $\text{Mn}_2\text{O}_3$ ) with Pearson symbol  $cI80$ , and the rhombohedral form (Corundum type like  $\text{Cr}_2\text{O}_3$ ) with Pearson symbol  $hR30$ . The rhombohedral modification is metastable under normal

conditions, but can be produced at high temperatures and pressures [17]. In the present work this modification has been ignored. The solubility of tin in the stable form of  $\text{In}_2\text{O}_3$  (Bixbyite) was investigated by Gonzalez and Mason [18], Ohya and Ito [19], Enoki and Echigoya [20], as well as Heward and Swenson [21] using different methods. All investigations are in general agreement and confirm a significant solubility of  $\text{SnO}_2$  in Bixbyite. In contrast, the solubility of zinc in Bixbyite appears to be relatively small. In the ternary  $\text{In}_2\text{O}_3$ - $\text{SnO}_2$ - $\text{ZnO}$  system Bixbyite is enriched with tin and zinc extending toward to the composition  $\text{ZnSnO}_3$  and can be described as  $\text{In}_{(2-2x)}\text{Sn}_x\text{Zn}_x\text{O}_3$  ( $0 < x < 0.40$ ) [1].

Bixbyite is described in this work as solid solution phase based on  $\text{In}_2\text{O}_3$  using the atomic sublattice model  $(\underline{\text{In}}, \text{Zn}, \text{Va})_1(\underline{\text{In}}, \text{Sn})_1(\text{O})_3$  assuming that the first and second sublattices can be occupied by metal atoms while the third contains oxygen atoms only. The atomic model is chosen, because the use of ions would require more additional unknown Gibbs energies to describe the solubility of tin oxide in Bixbyite. The molar Gibbs energy of this phase was expressed using the compound energy formalism [15, 16] as follows:

## Assessments

Thermodynamic descriptions for the binary metal systems are taken from the SGTE Solution database [13], the thermodynamic descriptions of binary metal-oxygen systems are proposed in this work. The data for the binary oxide systems  $\text{In}_2\text{O}_3$ - $\text{SnO}_2$ ,  $\text{In}_2\text{O}_3$ - $\text{ZnO}$  and  $\text{SnO}_2$ - $\text{ZnO}$  as well as the ternary system  $\text{In}_2\text{O}_3$ - $\text{SnO}_2$ - $\text{ZnO}$  are optimized using available experimental information. The calculated phase diagrams are in good agreement with the experimen-

$$G_m = y_{\text{In}}^I y_{\text{In}}^{\text{II}} {}^\circ G_{\text{In}_2\text{O}_3} + y_{\text{In}}^I y_{\text{Sn}}^{\text{II}} {}^\circ G_{\text{InSnO}_3} + y_{\text{Zn}}^I y_{\text{In}}^{\text{II}} {}^\circ G_{\text{ZnInO}_3} + y_{\text{Zn}}^I y_{\text{Sn}}^{\text{II}} {}^\circ G_{\text{ZnSnO}_3} + y_{\text{Va}}^I y_{\text{In}}^{\text{II}} {}^\circ G_{\text{InO}_3} + y_{\text{Va}}^I y_{\text{Sn}}^{\text{II}} {}^\circ G_{\text{SnO}_3} + (4) \\ + RT(y_{\text{In}}^I \ln y_{\text{In}}^I + y_{\text{Zn}}^I \ln y_{\text{Zn}}^I + y_{\text{Va}}^I \ln y_{\text{Va}}^I) + RT(y_{\text{In}}^{\text{II}} \ln y_{\text{In}}^{\text{II}} + y_{\text{Va}}^{\text{II}} \ln y_{\text{Va}}^{\text{II}}) + G_m^{\text{ex}}$$

where  $y_i^I$  and  $y_i^{\text{II}}$  represent the site fractions of the component  $i$  and  $j$  in the first respectively second sublattices.  ${}^\circ G_{\text{In}_2\text{O}_3}$  corresponds to the Gibbs energy of the indium oxide and is taken from the SGPS database [12], the Gibbs energy  ${}^\circ G_{\text{InO}_3}$  is estimated to be one half of the Gibbs energy of the appropriate oxide  $\text{In}_2\text{O}_3$ .

${}^\circ G_{\text{ZnSnO}_3}$  is the Gibbs energy of the hypothetical compound  $\text{ZnSnO}_3$ , while the Gibbs energies for the also hypothetical compounds  ${}^\circ G_{\text{InSnO}_3}$  and  ${}^\circ G_{\text{ZnInO}_3}$  could be estimated using the following reciprocal equation

$${}^\circ G_{\text{In}_2\text{O}_3} + {}^\circ G_{\text{ZnSnO}_3} = {}^\circ G_{\text{InSnO}_3} + {}^\circ G_{\text{ZnInO}_3} \quad (5)$$

and accepting that the species on the right-hand side have identical Gibbs energies

$${}^\circ G_{\text{InSnO}_3} = {}^\circ G_{\text{ZnInO}_3} = 0.5 \cdot {}^\circ G_{\text{In}_2\text{O}_3} + 0.5 \cdot {}^\circ G_{\text{ZnSnO}_3} \quad (6)$$

tal data. The thermodynamic data for the ternary compounds assessed in this work are given in Table 2. The Gibbs energies of  $(\text{Me}_1\text{O}_x)_A(\text{Me}_2\text{O}_y)_B$  have been based on stoichiometric combinations of  $\text{Me}_1\text{O}_x$  and  $\text{Me}_2\text{O}_y$  using a Neumann-Kopp approach. The values for  $\Delta H_{298}^0$  and  $S_{298}^0$  have been assessed according to available experimental data.

The end-member Gibbs-energies  $G^\circ$  as well as the various binary and ternary



interaction parameters between species both in the liquid and solid solutions have been assessed in order to obtain correct representations of the solubility regions. The optimization of the chosen solution

## Results and discussion

### The metallic subsystems

As indicated above, the data for the three metallic subsystems have been taken from the SGTE Solution database [13]. The resulting binary phase diagrams as well as the ternary liquidus surface are given below for reasons of completeness.

### The In-O system

The binary In-O system contains one stoichiometric compound,  $\text{In}_2\text{O}_3$ . The crystal structure of stable Indium oxide is the cubic form (Bixbyite type), whereas the rhombohedral modification (Corundum type) is metastable. According to Schneider [24], the melting point of Bixbyite  $\text{In}_2\text{O}_3$  is  $1910 \pm 10$  °C.

The solubility of oxygen in liquid indium was investigated first by Fitzner and Jacob [25] in the temperature range 650–820 °C using a phase equilibration technique. Later investigations using different techniques [26, 27] did not confirm these results [25]. Otsuka, Sano and Kozuka [26] determined the solubility of oxygen using coulometric titrations and later Otsuka, Kozuka and Chang [27] have used an isopi-

estic equilibration technique. Both measurements are in good agreement and show lower solubility of oxygen in liquid indium than determined by Fitzner and Jacob [25].

Isomäki, Hämäläinen et al. [28] in their assessment of the In-O binary system used the experimental data Fitzner and Jacob [25] applying the ionic liquid model.

Figure 5 shows the calculated phase diagram of the In-O binary system calculated from the present database compared with the experimental melting temperature of  $\text{In}_2\text{O}_3$  [24]. Figure 6 shows the Indium-rich part of the phase diagram compared

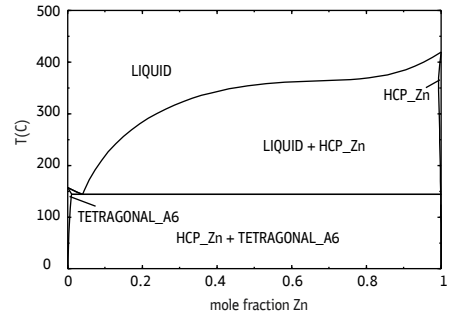


Fig. 2. Calculated In-Zn phase diagram

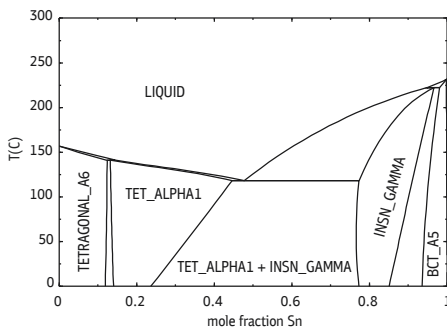


Fig. 1. Calculated In-Sn phase diagram

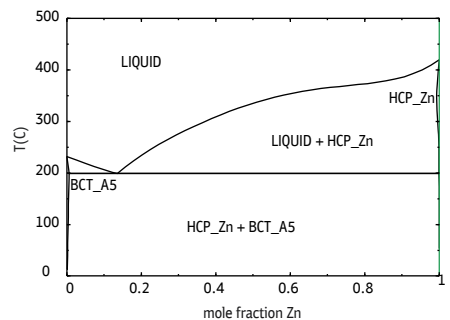


Fig. 3. Calculated Sn-Zn phase diagram



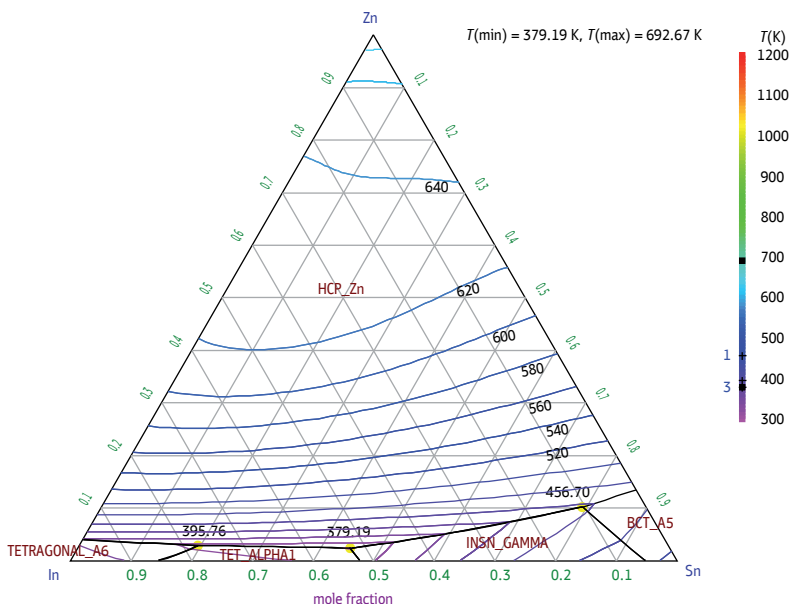


Fig. 4. Calculated liquidus surface in the In-Sn-Zn system

with the experiments [25–27], the agreement is very good.

### The Sn-O system

The Sn-O phase diagram used for the optimization was taken from Massalski [17], which is based on the experimental data reported by McPherson, Hansen [29] and Spandau, Kohlmeyer [30]. The system is characterized by a large region of liquid immiscibility between pure tin and “tin oxide” — rich compositions. The monotectic reaction between metal-rich and tin oxide-rich liquid is assumed to have a temperature of 1040 °C and liquid compositions of 3.3 and 50.3 at. % O according to [17]. It was confirmed by later investigations carried out by Cahen, David et al. [31] using DSC and XRD experiments.

The Sn-O binary system contains three intermediate compounds  $\text{SnO}$ ,  $\text{SnO}_2$  and  $\text{Sn}_3\text{O}_4$ . Although the experimentally determined melting temperatures of  $\text{SnO}_2$  vary enormously, all investigations agree that this compound melts congruently. Ac-

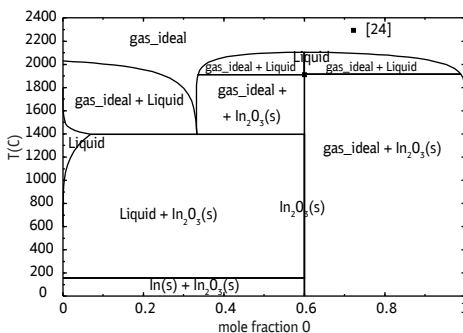


Fig. 5. Calculated In-O phase diagram

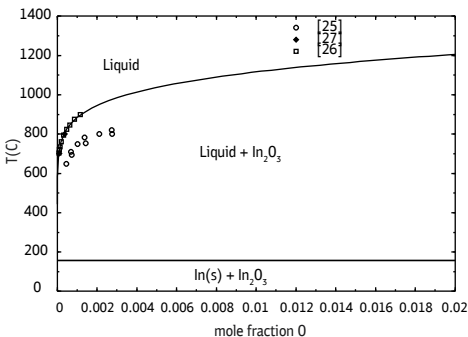


Fig. 6. Calculated phase equilibria in the In-rich part of the In-O diagram compared with experimental data [25–27]

According to [31] this compound melts congruently at 2000 °C in contradiction to the SGPS database [12] which gives a melting temperature of 1630 °C. In the present work the thermodynamic properties of pure SnO<sub>2</sub> were taken from [12]. Moh [32] have reported the existence of the compound SnO which is formed by a peritectoid reaction at 270 °C ( $\beta\text{Sn}$ ) + Sn<sub>3</sub>O<sub>4</sub> → SnO. Sn<sub>3</sub>O<sub>4</sub> is not stable at room temperature and decomposes at 450 °C [32].

A first thermodynamic assessment of the binary Sn-O system was given by Cahen, David et al. [31]. They assumed the melting temperature of SnO<sub>2</sub> to be 2000 °C and have modelled also the stoichiometric compounds SnO and Sn<sub>3</sub>O<sub>4</sub> using the thermal stabilities experimentally determined by Moh [32]. Later, a thermodynamic assessment was carried out by Isomäki, Hämäläinen et al. [28] where the thermodynamic data for SnO<sub>2</sub> were taken from the SGPS database [12] with the lower melting temperature of 1630 °C. The other two compounds were not considered in this work. In both assessments, the liquid phase was described using the ionic liquid model. In the assessment by Cahen [31], the entropies of formation for the compounds SnO and SnO<sub>2</sub> were determined to be 96.347 J/mol·K and 183.114 J/mol·K, respectively, which is in contradiction with the values published by Barin [33] (56.48 and 52.34 J/mol·K) and also the SGPS database [12] (57.17 and 49.01 J/mol·K).

In the present work the thermodynamic data for SnO<sub>2</sub> were taken from the SGPS database [12]. Also, the heat capacity of the compound SnO was taken from this source. The heat of formation of SnO determined by Li-Zi et al. [34] (-285920 J/mol) was used for the optimization combined together with the phase diagram data [32]. The assessed value is -289853 J/mol, the

difference to the measured value being about 1.37%. Sn<sub>3</sub>O<sub>4</sub> is modeled to be stable till 450 °C according to the experimental value of 450 °C [32].

The calculated Sn-O phase diagram is presented in Figure 7 compared with available experimental information; the agreement is good.

### The Zn-O system

For the binary Zn-O system no phase diagram is available. The information on this system including thermodynamics and structure of ZnO has been summarized by Wriedt [35]. The system contains one stoichiometric compound ZnO with known melting temperature (1972 °C) [17] but unknown melting behavior. No solubility of oxygen in pure zinc was reported. The binary Zn-O phase diagram resulting from the present dataset is shown in Figure 8 compared with the experimental data given in [17].

Zinc monoxide decomposes congruently by sublimation to the gaseous elements according to the following reaction:  $\text{ZnO(s)} \rightleftharpoons \text{Zn(g)} + 0.5\text{O}_2\text{(g)}$ .

The sublimation/vaporization of zinc oxide has been investigated by Knudsen Effusion Mass-spectroscopy (KEMS) [36–39]. At temperatures below 1500 K the vapor above ZnO consists almost exclusively

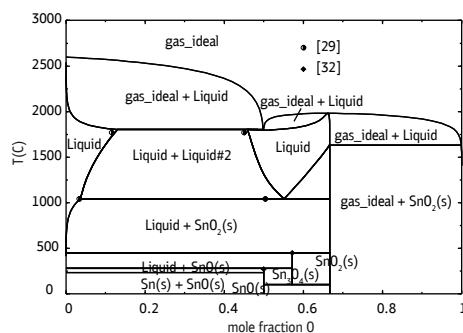


Fig. 7. Calculated Sn-O phase diagram compared with experimental data [29, 32]

of Zn atoms and  $O_2$  molecules, which confirms the congruent vaporization of ZnO. The oxygen partial pressure, which could not be measured correctly in the experiment, was estimated in agreement with the congruent sublimation condition by the above reaction as  $P(O_2) = 1/2 \cdot P(Zn)$ . Under the conditions of gas phase effusion from the cell, this relation takes the form  $P(O_2) = 1/2[M(O_2)/M(Zn)]^{1/2} \cdot P(Zn)$ , where  $M(O_2)$  and  $M(Zn)$  designate the oxygen and zinc molar masses. The sublimation enthalpy can be obtained from the temperature dependence of  $P(Zn)$  [38, 39] or calculated using the third-law [39]. The latter value is considered as more exact.

The selected data on the partial pressure of atomic Zn from the literature [37–41] are presented in Figure 9 (points and dashed lines) compared with the present equilibrium calculations (solid lines).

The deviation between the experimental datasets is notable especially in case of oxygen. It should be noted that the thermodynamic data for pure Zn, ZnO,  $O_2$  were taken from the SGTE databases [11, 12] without changes. Therefore, the discrepancy can be explained by differences with respect to both the thermodynamic data of individual gaseous species and the sublimation enthalpy of ZnO. For this, a value of 465.66 kJ/mol is used in the SGPS database. It is, however, in good agreement with the literature, i.e. 461.9 (via third-law calculations in [39]) or 467.66 in [37, 38].

### The Me1-Me2-O systems

Predicted isothermal sections at 500 °C for the ternary In–Sn–O, In–Zn–O and Sn–Zn–O systems are given in Figures 10–12. The pseudo-binary systems  $In_2O_3$ – $SnO_2$ ,  $SnO_2$ –ZnO and  $In_2O_3$ –ZnO are considered as a part of the corresponding systems Me1–Me2–O. It should be noted

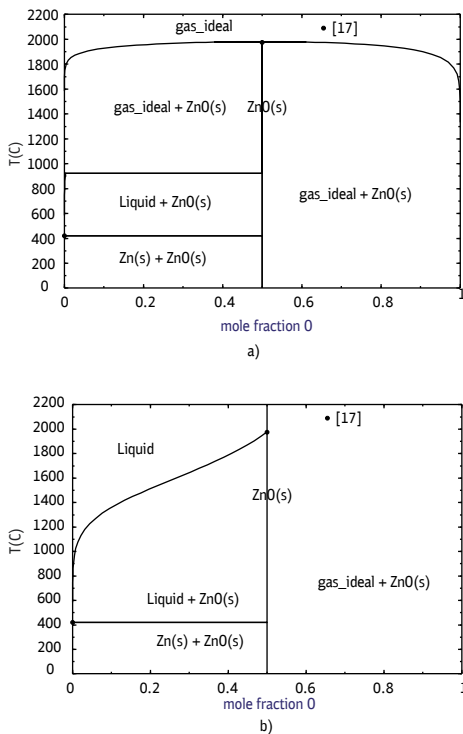


Fig. 8. Calculated Zn–O phase diagram: *a* — with participation of the gas phase, *b* — without

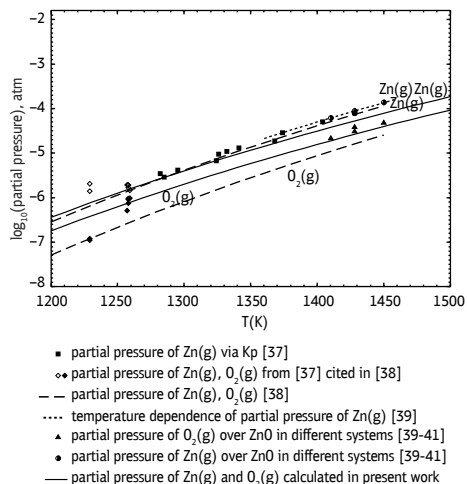


Fig. 9. Partial pressure of Zn and  $O_2$  over ZnO: comparison of literature data (points, dashed, dotted lines) with calculations solid (lines)

that the data for the ternary metallic system In-Sn-Zn and its binary subsystems were taken from the SGTE alloy database [13] and are not given in this paper. Only in the liquid metal phase a small solubility of O is calculated from the present data.

The behaviour of the respective systems along the oxide pseudo-binary systems is discussed below.

### The $\text{In}_2\text{O}_3$ - $\text{SnO}_2$ system

The pseudo binary system  $\text{In}_2\text{O}_3$ - $\text{SnO}_2$  is characterized by the presence of two intermediate phases stable at high temperatures, a significant solubility of tin in indium oxide and a eutectic reaction close to the tin-rich side. The system was investigated by Enoki and Echigoya [20] between 1200 and 1600 °C by TEM observations. Heward and Swenson [21] studied the phase diagram in the temperature range 1000–1650 °C using electron probe microanalysis (EPMA) and X-Ray diffraction (XRD) analysis of solid-state sintered samples. The solubility ranges of tin oxide in Bixbyite solid solution were investigat-

ed by Ohya, Ito et al. [19], Gonzales and Mason [18] and Harvey [1]. The experimentally determined solubility limits and phase boundaries for the Bixbyite solid solution contradict each other. According to Heward and Swenson [21], the maximal solubility of  $\text{SnO}_2$  in  $\text{In}_2\text{O}_3$  was found to be 13.1 mol.% at 1650 °C, whereas Ohya [19] reported 5% at 1500 °C. In contrast, the solubility of indium in  $\text{SnO}_2$  appears to be negligibly small [18, 21], which differs from the phase diagram obtained by Enoki [20]. In the  $\text{In}_2\text{O}_3$ - $\text{SnO}_2$  system two intermediate compounds,  $\text{Sn}_3\text{In}_4\text{O}_{12}$  and  $\text{SnIn}_2\text{O}_5$ , were observed. Both are stable at high temperatures and decompose eutectoidally at 1325 and 1575 °C, respectively [21]. The stoichiometric compound  $\text{Sn}_3\text{In}_4\text{O}_{12}$  was reported to be stable at temperatures above 1300 °C [18, 20] but was not observed by Harvey [3] at 1275 °C. The data on the experimentally determined thermal stability of the compound  $\text{In}_4\text{Sn}_3\text{O}_{12}$  are collected in Table 4.

The In-Sn-O system has been thermodynamically modelled by Isomäki,

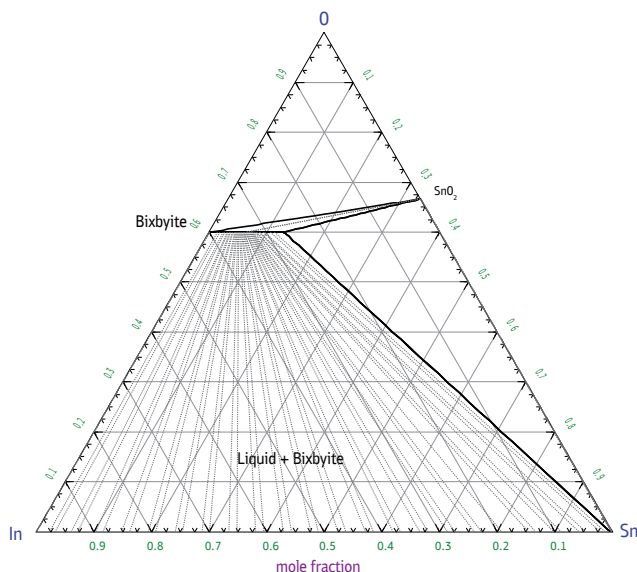


Fig. 10. The calculated In-Sn-O isothermal section at 500 °C

Hämäläinen et al. [28] who applied an ionic liquid two-sublattice model for the description of the liquid phase ( $\text{Sn}^{+2}$ ,  $\text{In}^{+3}$ ) ( $\text{SnO}_2, \text{O}^{-2}, \text{Va}$ ). Only one compound ( $\text{Sn}_3\text{I}$ -

$\text{n}_4\text{O}_{12}$ ) was modeled in this work, the solubility of tin in  $\text{In}_2\text{O}_3$  were optimized using the data of Enoki [20] which are significantly higher than those reported by Ohya

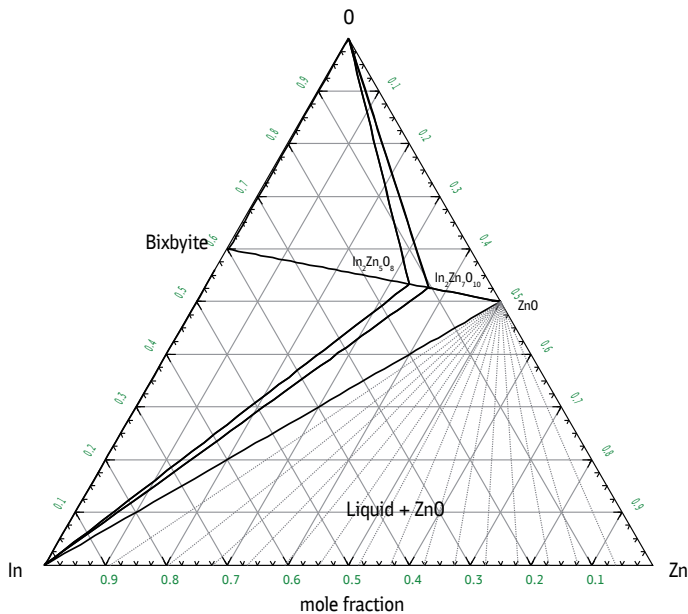


Fig. 11. The calculated In-Zn-O isothermal section at 500 °C

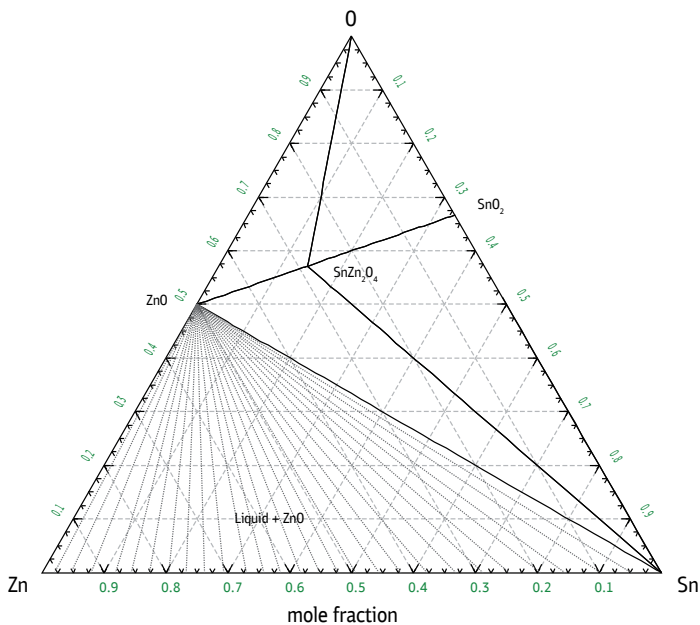


Fig. 12. The calculated Sn-Zn-O isothermal section at 500 °C

[19], Harvey [1] and Gonzalez [18]. The values by Enoki [20] were not used for the optimization in the present work. The calculated  $\text{In}_2\text{O}_3$ - $\text{SnO}_2$  binary system in air is presented in Figure 13 compared with the experimentally determined phase boundaries. The tin solubility in  $\text{In}_2\text{O}_3$  increases with temperature and reaches 4.6 at. % at 1730 °C. The system contains furthermore two intermediate high-temperature compounds  $\text{Sn}_3\text{In}_4\text{O}_{12}$  and  $\text{SnIn}_2\text{O}_5$ , the transition temperatures of which could be taken from the literature [20, 21, 42].

The calculated decomposing temperature of  $\text{Sn}_3\text{In}_4\text{O}_{12}$  is 1333 °C, very close to the experimental values 1325 [21] and 1335 °C [18] while the calculated  $T_2$ -temperature (1646 °C) agrees well with the experimental data by [21] and [42].

### The $\text{In}_2\text{O}_3$ -ZnO system

In the pseudo-binary system  $\text{In}_2\text{O}_3$ -ZnO Kasper [43] found that zinc oxide and indium oxides reacted at 1100 °C with formation of a series of homologous oxides  $\text{In}_2\text{Zn}_k\text{O}_{k+3}$  where  $k = 2-5$  and 7. Based on high-resolution electron microscopy results, Cannard and Tilley [44] proposed that the structures consist of  $k$  ZnO layers separated by two  $\text{InO}_{1.5}$  layers. ZnO has the wurtzite structure,  $\text{In}_2\text{O}_3$  crystallizes in the cubic bixbyite structure, and these two structures intergrow along the hexagonal  $c$ -axis direction. According to [44], at high ZnO concentrations  $\text{In}_2\text{Zn}_k\text{O}_{k+3}$  form com-

positions with  $k = 4-11$  at 1100 °C. Later, Nakamura [45] and Kimizuka [46] suggested that the compounds are isostructural with  $\text{LuFeO}_3(\text{ZnO})_k$ . Although the two models are not identical, both exhibit wurtzite-type layers perpendicular to the  $c$ -axis of the  $\text{In}_2\text{Zn}_k\text{O}_{k+3}$  structures. Compounds with  $k = 3-11, 13, 15, 17, 19$  were characterized by Nakamura [45, 47] using XRD and scanning electron microscopy (SEM). Moriga et al. [6] presented the sub-solidus phase diagram for the system  $\text{In}_2\text{O}_3$ -ZnO over the temperature range 1100–1400 °C. Homologous compounds  $\text{In}_2\text{Zn}_k\text{O}_{k+3}$  with  $k = 3-7, 9, 11, 13,$  and 15 were reported based on XRD. At 1100 °C,  $\text{In}_2\text{Zn}_5\text{O}_8$  and  $\text{In}_2\text{Zn}_7\text{O}_{10}$  only were found to be stable along with ZnO and  $\text{In}_2\text{O}_3$ , whereas the number of stable compounds increased as the temperature increased.

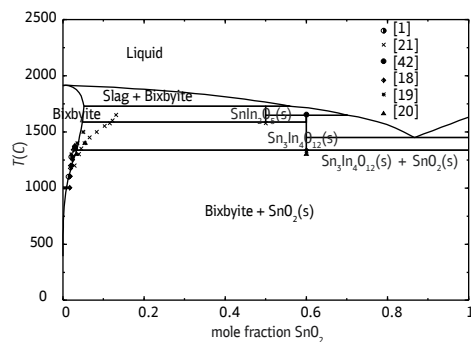


Fig. 13. The calculated  $\text{In}_2\text{O}_3$ - $\text{SnO}_2$  phase diagram in air compared with experimental data [1, 18–21, 42]

Table 4

Thermal stability of ternary stoichiometric compound  $\text{Sn}_3\text{In}_4\text{O}_{12}$

$T_1$ , °C	$T_2$ , °C	$T_1$ , °C in this work	$T_2$ , °C in this work
1300 Enoki [20]	–	1333	1646
1365 Ohya [19]	–		
1335 Gonzalez [18]	–		
1325 Heward [21]	1650 Heward [21]		
–	1652 Bates [42]		

The temperature ranges of stability determined in [6] agree with the previously reported information [43, 45, 46]. The difference was that the compounds with  $k = 4$  and 8 were not observed by Moriga [6] over the temperature range studied. Moreover, the presence of the compound with  $k = 15$  of the  $\text{In}_2\text{Zn}_k\text{O}_{k+3}$  series was almost impossible to detect with the XRD technique used in [6]. The formation of homologues series  $\text{In}_2\text{Zn}_k\text{O}_{k+3}$  (where  $k = 3-7, 9, 11$ ) was confirmed at 1275 °C in the study on the ternary system  $\text{In}_2\text{O}_3\text{-SnO}_2\text{-ZnO}$  [1], while the compounds with  $k = 6, 13, 15$  became stable at higher temperatures. The lattice constant, microstructure and electrical characteristics of  $\text{In}_2\text{O}_3$  ceramic doped by ZnO were investigated by Park et al. [48]. The solubility limit of ZnO in  $\text{In}_2\text{O}_3$  was reported to be close to 1 at.% when IZO (indium zinc oxide) was sintered in oxygen atmosphere. Sintering in nitrogen decreased the solubility limit to below 1 at.%.

No previous assessments on the system  $\text{In}_2\text{O}_3\text{-ZnO}$  were found in the literature. The present description of the system  $\text{In}_2\text{O}_3\text{-ZnO}$  is based on the data reported by Moriga [6]. The series of phases with the general formula  $\text{In}_2\text{Zn}_k\text{O}_{k+3}$  with  $k = 3-7, 9,$

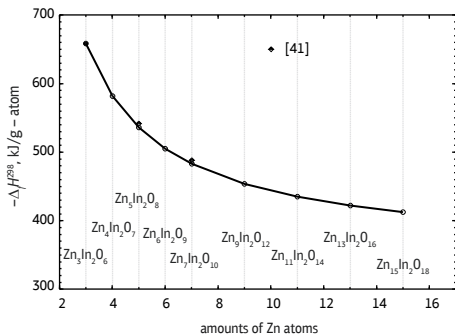


Fig. 14. Heat of formation of the stoichiometric compounds in the  $\text{In}_2\text{O}_3\text{-ZnO}$  system

11, 13, 15 was modelled in form of stoichiometric oxides. The thermodynamic data of these compounds are given in Table 2. Heat capacities of these compounds were generated according to Neumann — Kopp's rule based on the component oxides; the enthalpies and entropies of formation were optimized in accordance with the stability ranges of the phases. The formation enthalpy for the compounds with  $k = 5$  and 7 optimized in the present work are in very good agreement with those reported in [41] as shown in Figure 14. The literature data have been derived from a vaporization study of the system  $\text{In}_2\text{O}_3\text{-ZnO}$  with the KEMS technique. It is worth noting that all compounds show a very consistent trend with increasing content of Sn.

The solubility limit of ZnO in  $\text{In}_2\text{O}_3$  (bixbyite phase) was calculated at 1.56 mol.% and 1698 °C using the following atom-based model description of the phase:  $(\text{In}, \text{Zn}, \text{Va})_1(\text{In}, \text{Sn})_1(\text{O})_3$ . The liquid phase is assumed to consist of the component oxides,  $\text{Zn}_2\text{O}_2$  and  $\text{In}_2\text{O}_3$ , i.e. following the rule of two cations per molecule. The Gibbs energies of the stoichiometric homologous compounds are summarized in Table 2. The calculated phase diagram for the system  $\text{In}_2\text{O}_3\text{-ZnO}$

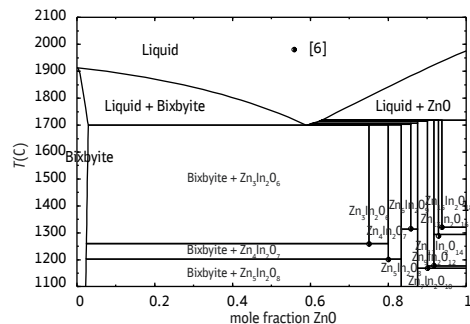


Fig. 15. The calculated  $\text{In}_2\text{O}_3\text{-ZnO}$  phase diagram in air compared with experimental data [6]



is presented in Fig. 15 compared with the experimental data [6].

### The SnO<sub>2</sub>-ZnO system

Enoki [49] proposed a preliminary phase diagram for the system SnO<sub>2</sub>-ZnO with the spinel phase only. The oxide mixtures were equilibrated at 1200 and 1400 °C and characterized by XRD. Most of the experimental studies [4, 49, 50] on this system agreed that there is one stable compound with the composition SnZn<sub>2</sub>O<sub>4</sub>. This compound has inverse spinel structure and can be obtained by solid state reaction from the component oxides or by decomposition of the salts zinc acetate (Zn(CH<sub>3</sub>COO)<sub>2</sub>) and tin tetrachloride (SnCl<sub>4</sub>). In contrast, the information on the second phase, ZnSnO<sub>3</sub>, is contradictory. Shen and Zhang [51] reported that this compound has a perovskite structure, whereas Inagaki [52] proposed an ilmenite structure which is more reasonable due to the fact that the ionic radius of Zn<sup>2+</sup> radius is too small to form a stable perovskite structure as has been confirmed later by Kovacheva and Petrov [53].

Palmer and Poeppelmeier [4] studied sub-solidus phase equilibria in the system Ga<sub>2</sub>O<sub>3</sub>-SnO<sub>2</sub>-ZnO at 1250 °C using solid state synthesis and XRD. The ZnO-SnO<sub>2</sub> binary system contains one intermediate compound, SnZn<sub>2</sub>O<sub>4</sub> with two-phase regions between the end-members and the spinel. According to [4], the lattice parameters of SnZn<sub>2</sub>O<sub>4</sub> were unchanged (from the nominal value) in two-phase mixtures with ZnO or SnO<sub>2</sub>, indicating minimal solubility of either oxide into the spinel phase. Hansson et al. [50] investigated phase equilibria for SnO<sub>2</sub>-ZnO system in air in the temperature range 1200 to 1400 °C using high-temperature equilibration and quenching techniques followed by electron probe X-ray microanalysis (EPMA). The maximum solubility of ZnO in SnO<sub>2</sub> was

found to be approximately 1.5 mol.% in the range of conditions investigated. The concentration of tin oxide in zincite (ZnO) is negligible between 1300 and 1400 °C in air within the limits of experimental uncertainty. A slight solubility of ZnO in the stoichiometric SnZn<sub>2</sub>O<sub>4</sub> spinel can be observed at all temperatures. Later Harvey et al. [1] did not observe a change of lattice parameter between pure ZnO or pure SnO<sub>2</sub> and doped compositions. Mihaiu et al. [54] undertook a systematic study of the phase formation over the whole compositional range of the ZnO-SnO<sub>2</sub> binary system in the temperature range 500–1500 °C. Starting with 900 °C, the formation of the SnZn<sub>2</sub>O<sub>4</sub> with inverse spinel type structure was found in all samples. The formation of the ZnSnO<sub>3</sub> was not observed under the experimental conditions used. In the temperature ranges 1000–1500 °C, no change in the phase composition was observed.

Vaporization processes in the ZnO-SnO<sub>2</sub> system have been studied by the Knudsen effusion technique in combination with mass spectrometric analysis (KEMS) of the vapor phase in the temperature range 1360 K to 1460 K [39]. Complete isothermal sublimation experiments have been performed to determine the partial pressures of vapor components over the whole system. The elemental composition of samples was quantified using laser mass spectrometry. By isothermal sublimation, the change of partial pressure of Zn over the system is caused by phase transformations in the solid state from pure ZnO through two heterogeneous fields (ZnO + Zn<sub>2</sub>SnO<sub>4</sub> and Zn<sub>2</sub>SnO<sub>4</sub> + SnO<sub>2</sub>) to pure tin oxide. It has been found that the gas phase mainly consists of Zn(g), O<sub>2</sub> and SnO(g). The partial pressures of the vapor species were determined at 1450 K.

In the present work, the compound  $\text{SnZn}_2\text{O}_4$  is treated as stoichiometric according to [3, 6] and calculated to be stable up to its melting point of 1675 °C. This compound is considered as the end-member constituent in the Spinel phase for the ternary system. The heat capacity of  $\text{SnZn}_2\text{O}_4$  was based on the data of the component oxides according to Neumann-Kopp (Table 2), the standard enthalpy of formation was optimized based on the experimental value from Gribchenkova [39]. The entropy was adjusted in order to represent the melting point of spinel. The compound  $\text{ZnSnO}_3$  was omitted from consideration according to literature data on its instability [39].

The liquid phase in the system  $\text{SnO}_2$ - $\text{ZnO}$  includes the associate  $\text{SnZn}_2\text{O}_4/1.5$  along with the basic oxides according to the modified associate species model. The melting properties of the spinel compound were based on those for liquid oxides. The two eutectics (Spinel and  $\text{ZnO}$  as well as Spinel and  $\text{SnO}_2$ ) are calculated at 1647 and 1425 °C, respectively. The calculated phase diagram of the system  $\text{SnO}_2$ - $\text{ZnO}$  is given in Figure 16.

The calculated activities across the system  $\text{SnO}_2$ - $\text{ZnO}$  at 1450 K are compared in Figure 17 with those measured in [39] using KEMS. The thermodynamic data

on the gas phase are taken from the SGPS database [12]. The following main gas species are found by calculation of equilibrium between the condensed phases and gas –  $\text{Zn}$ ,  $\text{SnO}$  and  $\text{O}_2$ .

The ratio between these species agreed with the measurements [39]; however, the absolute values of the partial pressures (especially for  $\text{Zn}$ ) differ from the experimental data due to scattering of experimental data on  $P(\text{Zn})$  obtained by using such a complicated method as KEMS. Moreover, the disagreement can be explained by possible small inconsistencies concerning the thermodynamic data of the gas components in the SGTE database, as was already mentioned above regarding the  $\text{Zn-O}$  system.

### The $\text{In}_2\text{O}_3$ - $\text{SnO}_2$ - $\text{ZnO}$ system

The ternary  $\text{In}_2\text{O}_3$ - $\text{SnO}_2$ - $\text{ZnO}$  system does not exhibit any ternary compounds, but presents two significant solid solution phases, the  $\text{SnZn}_2\text{O}_4$  Spinel phase enriched with indium with the formula  $\text{Zn}_{(2-x)}\text{Sn}_{(1-x)}\text{In}_{2x}\text{O}_4$  and the Bixbyite solid solution based on  $\text{In}_2\text{O}_3$  and extending far toward the  $\text{SnZnO}_3$  composition with the formula  $\text{In}_{(2-2x)}\text{Sn}_x\text{Zn}_x\text{O}_3$ . Palmer, Poppelmeier and Mason [55] studied the solid solubility of  $\text{ZnO}$  and  $\text{SnO}_2$  in Bixbyite at 1100 and 1250 °C using X-ray diffraction and determined a very strong coupled

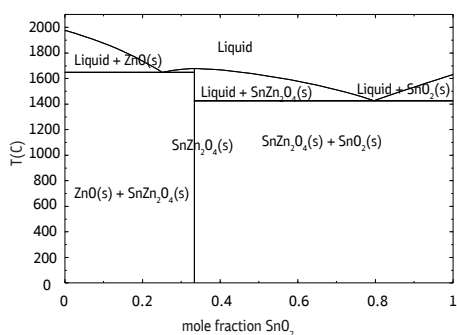


Fig. 16. Calculated  $\text{SnO}_2$ - $\text{ZnO}$  phase diagram in air

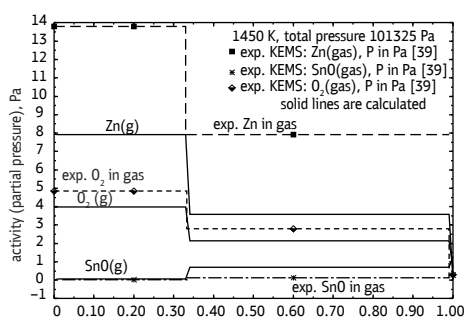


Fig. 17. Calculated and experimental activities in  $\text{SnO}_2$ - $\text{ZnO}$  system at 1450 K

solubility of  $\text{SnO}_2$  and  $\text{ZnO}$ . The maximum combined solubility of Zn and Sn can reach 40 cation %, the resulting material at this point can be described as  $\text{In}_{1.2}\text{Sn}_{0.4}\text{Zn}_{0.4}\text{O}_3$ . Later investigations by Kammler et al. [56] using X-ray powder diffraction confirmed high solubility of zinc and tin in  $\text{In}_2\text{O}_3$  at 1250 °C. Kammler reported also a wide spinel solution range,  $\text{Zn}_{2-x}\text{Sn}_{1-x}\text{In}_{2x}\text{O}_4$  ( $0 < x < 0.45$ ) and also a significant solubility of tin in  $\text{Zn}_3\text{In}_2\text{O}_6$  which was, however, not confirmed by later investigations [1, 2]. The phase diagram data published in [56] are constructed schematically and were not used for the present optimization work.

The present assessment of the ternary system is mainly based on the phase equilibria data published in [1]. Harvey, Poepelmeier and Mason [3] investigated the subsolidus phase relationships at 1275 °C using X-ray diffraction. They reported the existence of two extended solid solutions and preliminary phase relations between them and other coexisting compounds. Both solid solution phases exhibit constant Zn:Sn ratio and appear on the phase diagram as long vertical lines. The one significant solid solution phase is Bixbyite  $\text{In}_2\text{O}_3$ , enriched by tin and zinc, where up to 40% of indium can be replaced by tin and zinc. According to Harvey [1], the Bixbyite phase can be described using the formula  $\text{In}_{(2-2x)}\text{Sn}_x\text{Zn}_x\text{O}_3$ , where x can reach a maximum of 0.4. At 1275 °C, Bixbyite is in general in equilibrium with the Spinel phase, compound  $(\text{ZnO})_k(\text{In}_2\text{O}_3)$ , where

## Conclusions

A thermodynamic dataset containing all phases in the system  $\text{In}_2\text{O}_3$ - $\text{SnO}_2$ - $\text{ZnO}$  has been generated using the available experimental information (phase diagrams, phase transitions, structure, enthalpies of formation). The liquid and solid phases

$k = 3$ , and also with the tin oxide  $\text{SnO}_2$ . The other important solid solution phase reported by Harvey [1] is the Spinel phase, which extends from the binary composition  $\text{SnZn}_2\text{O}_4$  towards the  $\text{In}_2\text{ZnO}_4$  composition. Harvey confirmed Spinel phase boundaries and formula experimentally found by Kammler [56] to describe this indium-doped Spinel as  $\text{Zn}_{(2-x)}\text{Sn}_{(1-x)}\text{In}_{2x}\text{O}_4$  ( $0 < x \leq 0.45$ ), whereby at  $x = 0.45$  the Spinel composition corresponds to the formula  $\text{Zn}_{1.55}\text{Sn}_{0.55}\text{In}_{0.90}\text{O}_4$ . Harvey investigated also very intensively a zinc-oxide-rich region at 1275 °C and corresponding phase equilibria. As mentioned before, along the binary  $\text{ZnO}$ - $\text{In}_2\text{O}_3$  edge at 1275 °C there is a series of homologous compounds  $(\text{ZnO})_k(\text{In}_2\text{O}_3)$  (where  $k = 3-5, 7, 9, 11$ ), all of which are in equilibrium with the phase Spinel, starting with the first one  $(\text{ZnO})_{11}(\text{In}_2\text{O}_3)$  and finishing with the last  $(\text{ZnO})_3(\text{In}_2\text{O}_3)$  which is in equilibrium with Spinel maximally enriched in indium. The compounds with  $k > 11$  were not found in equilibrium with spinel at 1275 °C due to sluggish kinetics in the ZnO-rich composition range [1].

Figure 18 shows the calculated isothermal section at 1275 °C in the  $\text{InO}_{1.5}$ - $\text{SnO}_2$ - $\text{ZnO}$  system in air compared with experimental data [1]. The experimentally determined extensions of the solid solution phases Bixbyite and Spinel, the two-phase regions and also the compatibility triangles could be reproduced satisfactorily by the calculations.

have been introduced into the thermodynamic description, solid solution phases such as Spinel and Bixbyite have been modelled using the multi-sublattice approach. Fourteen stoichiometric compounds have also been thermodynamically assessed. The

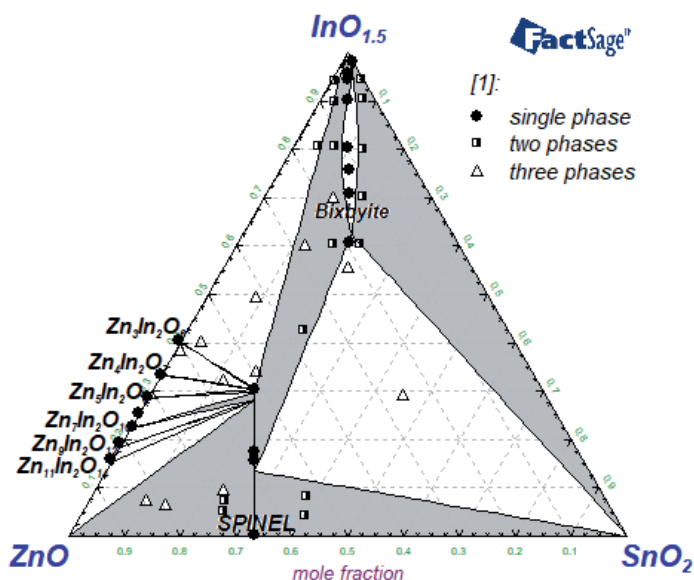


Fig. 18. Subsolidus phase relationships in  $\text{In}_2\text{O}_3$ - $\text{SnO}_2$ - $\text{ZnO}$  system in air at 1275 °C and 1 atm compared with experimental data [1]. Grey areas are the two-phase regions

liquid species tin (II, IV) oxides, indium and zinc oxides and the binary associate species ( $\text{SnZn}_2\text{O}_4$ ) have been introduced to the non-ideal associate solution. The general agreement between the calculated

phase equilibria as well as thermodynamic properties and the respective experimental data is good. The dataset can be applied to studies on the formation of ZITO-based TCOs.

## References

1. Harvey SP, Poepelmeier KR, Mason TO. Subsolidus Phase Relationships in the  $\text{ZnO}$ - $\text{In}_2\text{O}_3$ - $\text{SnO}_2$  System. *Journal of the American Ceramic Society*. 2008;91(11):3683-9. DOI: 10.1111/j1551-2916.2008.02686.x.
2. Hoel CA, Mason TO, Gaillard J-F, Poepelmeier KR. Transparent Conducting Oxides in the  $\text{ZnO}$ - $\text{In}_2\text{O}_3$ - $\text{SnO}_2$  System. *Chemistry of Materials*. 2010;22(12):3569-79. DOI: 10.1021/cm1004592.
3. Granqvist CG, Hultåker A. Transparent and conducting ITO films: new developments and applications. *Thin Solid Films*. 2002;411(1):1-5. DOI: 10.1016/S0040-6090(02)00163-3.
4. Palmer GB, Poepelmeier KR. Phase relations, transparency and conductivity in  $\text{Ga}_2\text{O}_3$ - $\text{SnO}_2$ - $\text{ZnO}$ . *Solid State Sciences*. 2002;4(3):317-22. DOI: 10.1016/S1293-2558(01)01258-4.
5. Minami T, Kakumu T, Takata S. Preparation of transparent and conductive  $\text{In}_2\text{O}_3$ - $\text{ZnO}$  films by radio frequency magnetron sputtering. *J Vac Sci Technol*. 1996;A14:1704-8. DOI: 10.1116/1.580323.

6. Moriga T, Edwards DD, Mason TO, Palmer GB, Poeppelmeier KR, Schindler JL, et al. Phase Relationships and Physical Properties of Homologous Compounds in the Zinc Oxide-Indium Oxide System. *Journal of the American Ceramic Society*. 1998;81(5):1310–6. DOI: 10.1111/j.1151-2916.1998.tb02483.x .
7. Besmann TM, Spear KE. Thermodynamic modelling of oxide glasses. *J Am Ceram Soc*. 2002;85(12):2887–94. DOI: 10.1111/j.1151-2916.2002.tb00552.x.
8. Yazhenskikh E, Jantzen T, Hack K, Müller M. Critical thermodynamic evaluation of oxide system relevant to fuel ashes and slags: Potassium oxide-magnesium oxide-silica. *Calphad*. 2014;47:35–49. DOI: 10.1016/j.calphad.2014.05.006.
9. Jantzen T, Hack K, Yazhenskikh E, Müller M. Evaluation of thermodynamic data and phase equilibria in the system Ca-Cr-Cu-Fe-Mg-Mn-S Part II: Ternary and quasi-ternary subsystems. *Calphad*. 2017;56:286–302. DOI: 10.1016/j.calphad.2017.01.007.
10. Jantzen T, Hack K, Yazhenskikh E, Müller M. Addition of TiO<sub>2</sub> and Ti<sub>2</sub>O<sub>3</sub> to the Al<sub>2</sub>O<sub>3</sub>-FeO-Fe<sub>2</sub>O<sub>3</sub>-MgO system. *Calphad*. 2018;62:187–200. DOI: 10.1016/j.calphad.2018.05.009.
11. SGTE unary database 2017.
12. SGPS — SGTE pure substances database (v13.1) 2017.
13. SGTE Solution database 2017.
14. Pearson WB. *A Handbook of Lattice Spacings and Structures of Metals and Alloys*. Oxford: Pergamon Press; 1967.
15. Hillert M, Staffansson L–I. Regular Solution Model for Stoichiometric Phases and Ionic Melts. *Acta Chem Scand*. 1970;24(10):3618–26. DOI:10.3891/acta.chem.scand. 24–3618.
16. Sundman B, Aagren J. A regular solution model for phases with several components and sublattices, suitable for computer applications. *J Phys Chem Solids*. 1981;42(Copyright (C) 2018 American Chemical Society (ACS). All Rights Reserved.):297–301. DOI: 10.1016/0022-3697(81)90144-x.
17. Massalski TB. *Binary Alloy Phase Diagrams*. Second ed. Metals Park, OH ASM International; 1990.
18. González GB, Mason TO, Okasinski JS, Buslaps T, Honkimäki V. Determination of the Solubility of Tin in Indium Oxide Using In Situ and Ex Situ X-Ray Diffraction. *J Am Ceram Soc*. 2011:1–7. DOI: 10.1111/j.1151-2916.2011.04999.x.
19. Ohya Y, Ito T, Kaneko M, Takahashi Y. Solid solubility of SnO<sub>2</sub> in In<sub>2</sub>O<sub>3</sub>. *J Ceram Soc Jpn*. 2000;108(9):803–6. DOI: 10.2109/jcersj.108.1261\_803.
20. Enoki H, Echigoya J, Suto H. The intermediate compound in the In<sub>2</sub>O<sub>3</sub>-SnO<sub>2</sub> system. *Journal of Materials Science*. 1991;26(15):4110–5. DOI: 10.1007/bf02402954.
21. Heward WJ, Swenson DJ. Phase equilibria in the pseudo-binary In<sub>2</sub>O<sub>3</sub>-SnO<sub>2</sub> system. *J Mater Sci*. 2007;42(Copyright (C) 2018 American Chemical Society (ACS). All Rights Reserved.):7135–40. DOI: 10.1007/s10853-007-1569-y.
22. FactSage: Facility for the Analysis of Chemical Thermodynamics. Montreal, Canada: CRCT-ThermFact Inc. and GTT-Technologies; 1976–2015; Available from: <http://www.factsage.com/>.

23. Bale CW, Bélisle E, Chartrand P, Deckerov SA, Eriksson G, Gheribi AE, et al. FactSage thermochemical software and databases, 2010–2016. *Calphad*. 2016;54:35–53. <http://dx.doi.org/10.1016/j.calphad.2016.05.002>.
24. Schneider SJ. Phase Equilibria in Systems Involving the Rare Earth Oxides. Part III. The  $\text{Eu}_2\text{O}_3$ - $\text{In}_2\text{O}_3$  System. *J Res Nat Bureau of Standards*. 1961;65A(5):429–34. DOI: 10.6028/jres.065A.044.
25. Fitzner K, Jacob KT. Solubility and activity of oxygen in liquid indium and copper-indium alloys. *Journal of the Less Common Metals*. 1977;52(2):279–91. DOI: 10.1016/0022-5088(77)90009-1.
26. Otsuka S, Sano T, Kozuka Z. Activities of oxygen in liquid thallium and indium from electrochemical measurements. *MTB*. 1980;11(2):313–9. DOI: 10.1007/bf02668417.
27. Otsuka S, Kozuka Z, Chang YA. Oxygen solubility in liquid indium and oxygen diffusivity in liquid indium and tin. *MTB*. 1984;15(2):329–35. DOI: 10.1007/bf02667336.
28. Isomäki I, Hämäläinen M, Gierlotka W, Onderka B, Fitzner K. Thermodynamic evaluation of the In–Sn–O system. *Journal of Alloys and Compounds*. 2006;422(1):173–7. DOI:10.1016/j.jallcom.2005.11.083.
29. McPherson DJ, Hansen M. The system Zirconium–Tin. *Trans ASM*. 1953;45:915–33.
30. Spandau H, Kohlmeyer EJ. Über Zinnmonoxyd und sein Verhalten bei hohen Temperaturen. *Z Anorg Chem*. 1947;254:65–82.
31. Cahen S, David N, Fiorani JM, Maître A, Vilasi M. Thermodynamic modelling of the O–Sn system. *Thermochimica Acta*. 2003;403(2):275–85. DOI: 10.1016/S0040-6031(03)00059-5.
32. Moh GH. Tin-containing mineral systems. I. Tin-iron-sulfur-oxygen system and mineral assemblages in ores. *Chem Erde*. 1974;33(Copyright (C) 2018 American Chemical Society (ACS). All Rights Reserved.):243–75.
33. Barin I. *Thermochemical Data of Pure Substances*: VCH Verlagsgesellschaft mbH; 1995.
34. Li-Zi Y, Zhi-Tong S, Chan-Zheng W. A Thermodynamic Study of Tin Oxides by Coulometric Titration. *Journal of Solid State Chemistry*. 1994;113(2):221–4. DOI: 10.1006/jssc.1994.1363.
35. Wriedt HA. The O–Zn (Oxygen–Zinc) system. *Journal of Phase Equilibria*. 1987;8(2):166. DOI: 10.1007/bf02873202.
36. Searcy AW. *High-Temperature Inorganic Chemistry*. *Progress in Inorganic Chemistry* 1962. DOI: 10.1002/9780470166048.ch2.
37. Anthrop DF, Searcy AW. Sublimation and Thermodynamic Properties of Zinc Oxide. *J Phys Chem*. 1964;68(8):2335–42. DOI: 10.1021/j100790a052.
38. Kazenas EK, Tsvetkov JV. *The evaporation of oxides*. Moscow: Nauka; 1997.
39. Gribchenkova NA, Steblevsky AV, Alikhanyan AS. Vaporization thermodynamics of the  $\text{ZnO}$ – $\text{SnO}_2$  system. *The Journal of Chemical Thermodynamics*. 2014;70:203–6. DOI: 10.1016/j.jct.2013.11.010.
40. Gribchenkova NA, Steblevsky AV, Alikhanyan AS. Vaporization in the  $\text{Ga}_2\text{O}_3$ – $\text{ZnO}$  system by high temperature mass spectrometry. *The Journal of Chemical Thermodynamics*. 2017;115:1–6. DOI: 10.1016/j.jct.2017.07.009.



41. Gribchenkova NA, Alikhanyan AS, editors. Mass spectrometric investigation of phase equilibria and thermodynamics of ZnO- $M_xO_y$  ( $M_xO_y = Ga_2O_3, In_2O_3, SnO_2$ ) quasi-binary oxide systems. Knudsen Effusion Mass Spectrometry, KEMS Workshop; 2017 October, 23–25; Jülich, Germany: Forschungszentrum Jülich.
42. Bates JL, Griffin CW, Marchant DD, Garnier JE. Electrical conductivity, Seebeck coefficient, and structure of indium(III) oxide-tin(IV) oxide. *Am Ceram Soc Bull.* 1986;65:673–8.
43. Kasper H. Neuartige Phasen mit wurtzitähnlichen Strukturen im System ZnO- $In_2O_3$ , *Zeitschrift für anorganische und allgemeine Chemie.* 1967;349(3-4):113–23. DOI: 10.1002/zaac.19673490302.
44. Cannard PJ, Tilley RJD. New intergrowth phases in the ZnO- $In_2O_3$  system. *Journal of Solid State Chemistry.* 1988;73(2):418–26. DOI: 10.1016/0022-4596(88)90127-2.
45. Nakamura M, Kimizuka N, Mohri T. The phase relations in the  $In_2O_3$ - $Fe_2ZnO_4$ -ZnO system at 1350°C. *Journal of Solid State Chemistry.* 1990;86(1):16–40. DOI: 10.1016/0022-4596(90)90110-J.
46. Kimizuka N, Isobe M, Nakamura M. Syntheses and Single-Crystal Data of Homologous Compounds,  $In_2O_3(ZnO)_m$  ( $m = 3, 4, \text{ and } 5$ ),  $InGaO_3(ZnO)_3$ , and  $Ga_2O_3(ZnO)_m$  ( $m = 7, 8, 9, \text{ and } 16$ ) in the  $In_2O_3$ - $ZnGa_2O_4$ -ZnO System. *Journal of Solid State Chemistry.* 1995;116(1):170–8. DOI: 10.1006/jssc.1995.1198.
47. Nakamura M, Kimizuka N, Mohri T, Isobe M. The Phase Relations in the  $In_2O_3$ - $Al_2ZnO_4$ -ZnO System at 1350°C. *Journal of Solid State Chemistry.* 1993;105(2):535–49. DOI: 10.1006/jssc.1993.1246.
48. Park D-H, Son K-Y, Lee J-H, Kim J-J, Lee J-S. Effect of ZnO addition in  $In_2O_3$  ceramics: defect chemistry and sintering behavior. *Solid State Ionics.* 2004;172(1):431–4. DOI: 10.1016/j.ssi.2004.03.029.
49. Enoki H. Oxide transparent electrode materials. *Materia.* 1995;34(3):344–51. DOI: 10.2320/materia.34.344.
50. Hansson R, Hayes PC, Jak E. Experimental study of phase equilibria in the Fe–Sn–Zn–O system in air. *Can Metall Q.* 2004;43(4):545–54. DOI: 10.1179/cm.2004.43.4.545.
51. Yu-Sheng S, Tian-Shu Z. Preparation, structure and gas-sensing properties of ultra-micro  $ZnSnO_3$  powder. *Sensors and Actuators B: Chemical.* 1993;12(1):5–9. DOI: 10.1016/0925-4005(93)85003-S.
52. Inagaki M, Kuroishi T, Yamashita Y, Urata M. Syntheses of  $M\text{Sn}(\text{OH})_6$  by coprecipitation and of  $M\text{SnO}_3$  by thermal decomposition ( $M = \text{Mg, Co, Zn, Mn, Cd, Ca, Sr, Ba}$ ). *Zeitschrift für anorganische und allgemeine Chemie.* 1985;527(8):193–202. DOI: 10.1002/zaac.19855270822.
53. Kovacheva D, Petrov K. Preparation of crystalline  $ZnSnO_3$  from  $Li_2SnO_3$  by low-temperature ion exchange. *Solid State Ionics.* 1998;109(3):327–32. DOI: 10.1016/S0167-2738(97)00507-9.
54. Mihaiu S, Atkinson I, Mocioiu O, Toader A, Tenea E, Zaharescu M. Phase formation mechanism in the ZnO- $SnO_2$  binary system. *Rev Roum Chim.* 2011;56(5):465–72.
55. Palmer GB, Poepfelmeier KR, Mason TO. Conductivity and Transparency of ZnO/ $SnO_2$ -Cosubstituted  $In_2O_3$ . *Chem Mater.* 1997;9 (Copyright (C) 2018 American Chemical Society (ACS). All Rights Reserved.):3121–6. DOI: 10.1021/cm9704037.



56. Kammler DR, Edwards DD, Ingram BJ, Mason TO, Palmer GB, Ambrosini A, et al. Novel Compound and Solid-Solution Transparent Conducting Oxides for Photovoltaics. In: V. K. Kapur RDM, D. Carlson, G. P. Ceasar, A. Rohatgi, editor. *Electrochem Soc 195th Meeting: Photovoltaics for the 21st Century*; Seattle, Washington. Pennington, New Jersey: The Electrochemical Society, Inc., 1999. P. 68–77.